

RESEARCH ARTICLE

The impact of clot permeability on platelet fluxes toward its surface

Niksa Mohammadi Bagheri¹, Gabor Závodszky, Alfons G. Hoekstra*

Computational Science Lab, Informatics Institute, Faculty of Science, University of Amsterdam, Amsterdam 1098 XH, The Netherlands

* a.g.hoekstra@uva.nl



Abstract

Platelet aggregation is regulated by a series of chemical reactions that control platelet adhesion on a thrombogenic surface. These reactions are influenced by the complex interaction between reaction kinetics and hemodynamics. This study systematically investigates the transport of platelets, considering the interaction between flow-mediated mass transfer mechanisms and reaction kinetics as a function of clot permeability. A two-dimensional finite element model is developed to replicate static blood flow, platelet transport, and adhesion on a semi-elliptical and semi-circular structure representing permeable clots. The platelet-clot interface interactions are extensively investigated using a hindered transport model, focusing on clot permeabilities, reaction rates, and flow conditions. In the case of clots with highly reactive surfaces, an increase in clot permeability can lead up to four-fold increase in total platelet flux compared to non-permeable clots due to differences in transport environments.

OPEN ACCESS

Bagheri NM, Závodszky G, Hoekstra AG (2025) The impact of clot permeability on platelet fluxes toward its surface. PLoS ONE 20(3): e0317828. <https://doi.org/10.1371/journal.pone.0317828>

Editor: James P. Maloney, University of Colorado - Anschutz Medical Campus, Internal Medicine, 12700 E. 19th Ave, C272; Pulmonary, UNITED STATES OF AMERICA, Aurora, Colorado, 80045

Received: May 08, 2024

Accepted: January 06, 2025

Published: March 25, 2025

Copyright: © 2025 Bagheri et al. This is an open access article distributed under the terms of the [Creative Commons Attribution License](https://creativecommons.org/licenses/by/4.0/), which permits unrestricted use, distribution, and reproduction in any medium, provided the original author and source are credited.

Data availability statement: All relevant data are within the manuscript and its [Supporting Information](#) files.

Funding: This study was supported by the European Commission through the H2020 project 'In Silico World: Lowering barriers to ubiquitous adoption of In Silico Trials' (topic SC1-DTH-06-2020, grant ID 101016503). The funders had no role in study design, data

1 Introduction

In response to vessel injury, platelets aggregate on the damaged thrombogenic surface, creating a permeable structure that facilitates the coagulation cascade and subsequent fibrin generation [1]. Platelet aggregate formation is a multi-faceted phenomenon mainly involving interactions between red blood cells, platelets, plasma proteins, and injured areas [2]. In particular, blood agonists and flow conditions [3,4] are critical factors that dictate specific thrombus composition and formation mechanisms [5,6]. Shear-induced platelet aggregates (SIPAs) [7] are characterized as permeable clots that arise from the combination of pathologic flows and sufficient concentrations of von Willebrand factor (vWF). The vWF is pivotal in promoting the platelet deposition rate by increasing platelet adhesion [8]. Thrombi can also form in backward-facing step (BFS) geometries [9] under low-flow velocity conditions and recirculation zones, leading to high concentrations of potentially activated platelets, which experience low shear stress and long residence times [10]. These areas give rise to dense accumulations of platelets and fibrin in combination with considerably lower clot permeabilities [11]. In such scenarios, platelet binding and deposition occur due to local regions experiencing a spatially or temporally induced micro shear rate gradient [12] that reaches a certain threshold [13].

Platelets are carried toward the surface of a clot through advection and diffusion [14]. Hemodynamics can also initiate diverse reaction kinetics [15,16], resulting in distinct

collection, and analysis, decision to publish, or preparation of the manuscript.

Competing interests: The authors have declared that no competing interests exist.

thrombosis scenarios. Hence, by creating an environment that is either transport-dominated or reaction-dominated [17], particularly within the region where the clot is forming [18], a unique growth rate and pattern may emerge. Tokarev et al. [19] computed the platelet flux towards the vessel wall by incorporating Smoluchowski's theory, accounting for parameters like near-wall shear rate, collision frequency, and collision efficiency. An earlier study [20] showed that the stochasticity of platelet adhesive interactions in relation to localized flow changes plays an essential role in specifying the dynamics of the arterial thrombus shell and thrombus growth pattern [3]. It is important to note that the dynamic and static behavior of platelets and plasma proteins at the surface of a thrombus may be affected by the varying porous structure of the growing clot, thereby either intensifying or hindering the thrombosis process [21].

Blood thrombi have been characterized as heterogeneous structures, comprising a densely packed platelet core surrounded by an outer shell of loosely bonded platelets with higher permeability and dynamic behavior [22,23]. This outer layer, with its poro-viscoelastic behavior [24], significantly impacts the collision, adhesion, and embolization patterns of platelets [25]. The presence of porous structures has the potential to significantly modify flow characteristics, which, in the context of a clot, can directly influence its stability [24]. In the process of clot retraction, platelets are brought into proximity, and much of the fluid between them is expelled. As mentioned by Leiderman et al. [26], older thrombi exhibit substantially reduced porosity compared to freshly formed clots, with the study indicating a six-fold decrease in permeability for aged clots of similar composition compared to newly formed clots. According to [27], older arterial thrombi contain more fibrin fibers and fewer intervening pores, which increases clot density and may reduce thrombus permeability. Studies have reported a wide range of clot permeabilities [11,28–35], with values varying by up to seven orders of magnitude. These variations are influenced by factors such as blood flow dynamics, clot composition, and the presence or type of anticoagulants. This raises the question of why there is significant variation in permeabilities and how this parameter influences clot initiation and formation.

In analyzing the physical aspect of platelet arterial thrombosis, Du et al. [11] designed high-shear flow experiments, investigating the growth of platelet-rich white clots. Their findings revealed that the permeability of a white clot is three orders of magnitude higher than that of a red clot. Additionally, it was shown that integrating the lower reported permeabilities by others leads to an insufficient formation of interplatelet bonds, ultimately resulting in early disintegration of the thrombus.

Kim and Ku [36] reported that the presence of pores in transverse sections of a SIPA clot suggests high permeability, where this high permeability facilitates convective transport of drugs through the inner portion of the clot. On the other hand, the hindrance caused by low clot permeabilities could introduce restrictions on availability of both platelet agonists and coagulation products [21]. Muthard and Diamond [37] examined intra-thrombus permeation under controlled pressure drops in a microfluidic setup. Their findings quantitatively estimated the contracted clot permeability and the associated transport of ADP and TXA2 within the clot. According to their findings, a reduced ADP/TXA2 transport rate may also contribute to forming a dense inner thrombus core. To better understand the critical role of platelets in forming permeable clots, it is vital to investigate the underlying reasons that impact their exposure time [38] and binding rate [39] to the sub endothelium and other platelets.

The initial stages of platelet aggregate formation involve primary adhesion, followed by platelet rolling at the clot surface, which may lead to stable adhesion if platelet activation has enough time [7]. As the thrombus grows, the platelet rolling velocity increases due to the

hydrodynamic force exerted on the platelets at the thrombus surface [7]. This gradual change in platelet adhesiveness leads to only a portion of platelets firmly attaching to the growing thrombus. As a result, the growth of thrombus may be limited by the capacity of platelets to transfer to the interface and adhere when the aggregate height exceeds a critical threshold [20]. So far, most theoretical models [40–43] center on platelets as chemical entities with generalized cohesive strength and binding rate, which affect the flow domain through high viscous forces in a growing region of low permeability. This approach neglects the interdependence between the distinctive permeable nature of the clots and the local fluid dynamics, especially in the shell zones of thrombus [44], in defining the impact of binding kinetics on aggregate formation. Further exploration of the interplay between binding kinetics and transport of platelets, permeabilities of clots, and hemodynamics is needed.

A recent study by Zhussupbekov et al. [45] examined the influence of surface chemistry and shear rate on thrombosis in micro-cervices. They hypothesize that this phenomenon can be attributed to the equilibrium between platelet deposition pattern and clearance. It was stated that the presence or absence of a prominent recirculation zone is believed to be the reason behind the different effects of flow rate on clot growth in various crevices. Nonetheless, to the authors' knowledge, no research has been conducted on how variations in clot permeability and platelet adhesion chemistry affect the spatial and temporal behavior of platelets around an expanding clot in relation to hemodynamics. This study comprehensively investigates the correlation between flow-mediated and reaction-mediated mass transfer mechanisms in dictating platelet transport and deposition patterns through a mathematical framework of hindered transport of platelets. In contrast with chemical agonists, we assume that platelets can be transported toward the clot surface and may react on the clot surface but are not able to be transported into the clot, as pore sizes are probably too small to allow inter-thrombus platelet transport. This critical distinction between platelets and other relevant agonists has yet to be addressed in detail. A systematic two-dimensional numerical benchmark model is presented for simulating blood flow, platelet mass transport, and platelet adhesion to a clot surface. The model utilizes a permeable semi-circle/ellipsoid structure to represent typical generic permeable aggregate shapes in a two-dimensional domain. The model includes a specific semi-permeable boundary condition on the clot surface that allows free flow but prevents platelets from being transported into the clot. First, the specific flow patterns that govern the transportation of platelets as a function of varying hemodynamics and clot permeability ranges are studied. Then, the relationship and significance of platelet binding rates are undertaken to investigate its impact on platelet transport behavior within a thrombus's outer layers. Platelet flux toward the surface is studied in detail to evaluate the impact of clot permeability on platelet transfer and distribution behavior surrounding a permeable clot.

2 Methodology

The central focus of this study is to investigate the adhesion of platelets to a permeable boundary layer of the clot, which is influenced by platelet advection and diffusion flux as well as chemical reactions. The adhesion process is assumed to depend on the flux in the normal direction to the clot boundary layer [47,48].

A two-dimensional flow channel of length L and height H is created (see Fig 1). A parabolic inlet velocity is assumed. At the outlet, a free flow condition is assumed. Midway the channel at the lower wall, a clot with homogeneous porosity ε and related permeability κ is situated with length l and height h . We consider a half-circle shape ($l = h$) and a half-elliptic shape (with $l = 2h$) as representations of a simplified clot shape, based on the actual thrombus

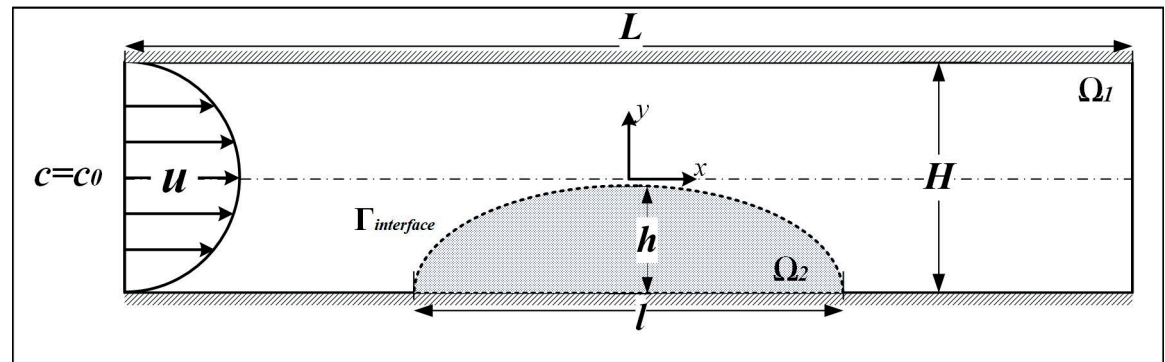


Fig 1. The simulation domain.

<https://doi.org/10.1371/journal.pone.0317828.g001>

shapes observed in previous studies [18,23,32,49]. A domain blockage ratio is defined as $\beta = \frac{h}{H}$. At the inlet, a homogeneous platelet concentration c_0 is assumed.

The steady-state flow of an incompressible Newtonian fluid with density ρ and viscosity μ is computed, where the effect of the porous clot domain is modeled with a body force using the Darcy-Brinkman-Forchheimer model [50]. The model was chosen for its ability to account for both viscous shear and inertial effects, offering a more accurate representation of flow dynamics around thrombi. This model surpasses the simpler Darcy law by capturing non-linear resistance under complex hemodynamic conditions. The steady-state incompressible Navier-Stokes equations are expressed in dimensionless form:

$$\nabla \cdot \vec{u} = 0, \quad (1)$$

$$\frac{1}{\varepsilon^2} (\vec{u} \cdot \vec{\nabla}) \vec{u} = -\nabla(p) + \frac{1}{\varepsilon Re} \nabla^2 \vec{u} - \frac{1}{Re Da} \vec{u} - \frac{c_F}{\sqrt{Da}} |\vec{u}| \vec{u}, \quad (2)$$

where \vec{u} and p are the dimensionless velocity and pressure defined as $\vec{u} = \frac{\vec{u}^*}{U_\infty}$ and $p = \frac{p^*}{\rho U_\infty^2}$. The superscript $*$ is employed to signify dimensional variables, and U_∞ is the mean inlet velocity. In these equations, spatial coordinates are scaled by a characteristic length h , and the gradient operator ∇^* is transformed as $\nabla = \frac{1}{h} \nabla^*$. Re and Da are the Reynolds and Darcy number, respectively, defined as $Da = \frac{\kappa}{h^2}$ and $Re = \frac{\rho U_\infty h}{\mu}$. C_F is the Forchheimer coefficient, $C_F = \frac{1.75}{\sqrt{150\varepsilon^3}}$. Note that in flow domain Ω_1 (outside the clot) the terms representing this body force are zero, and the last two terms in Eq. 2 drop out (stated differently, in the free flow domain Ω_1 one could say that $Da = \infty$ and $\varepsilon = 1$ resulting in the standard Navier-Stokes equations outside the clot).

The accurate relationship between the porosity (ε) and the permeability (κ) of the clot is not fully known [11]. However, it is known that within the expected range of porosities (0.3–0.7) [32], the resulting permeabilities exhibit significant changes across several orders of magnitude. Accordingly, in this study, the primary influence of clot porous structure on the flow inside the clot is investigated by dimensionless permeability (Da), following similar previous frameworks [51,52], suggesting that the main effect on the flow inside the clot is through the Da in the body force (Brinkman and Forchheimer drag term), with minor impact of porosity. In Ω_2 we kept $\varepsilon = 0.7$ in the flow simulations while sweeping over the Da ranges.

The transport of the platelets is modeled via the advection-diffusion equation ($\Omega 1$), where we again assume a steady state, assume an isotropic and constant platelet diffusivity D , and express the advection-diffusion equations in dimensionless form:

$$\vec{u} \cdot \nabla c = \frac{1}{Pe} \nabla^2 c, \quad (3)$$

where $c = \frac{c^*}{c_0}$ is the dimensionless concentration of platelets in the fluid and c_0 the platelet concentration at the inlet. The Peclet number is defined as $Pe = \frac{U_\infty h}{D}$. Finally, the boundary conditions for the advection-diffusion equation need to be specified. The walls of the channel are inert, which is achieved by setting the normal flux of platelets on the wall to zero, $\vec{n} \cdot \left(c\vec{u} - \frac{1}{Pe} \nabla c \right) = 0$, where \vec{n} is the surface normal vector. This boundary condition is also applied to the surface of the clot. Combined with an initial condition setting $c = 0$, except at the inlet, the boundary condition will act on the clot surface as a semi-permeable boundary condition, preventing platelets from entering the clot volume. However, platelets can react with the surface, where they are adsorbed, removing platelets from the solution and effectively resulting in a platelet flux towards the surface that should be included in the boundary condition. The Langmuir adsorption model is employed, where we assume that the concentration of bounded platelets on the clot surface c_s is minimal, keeping the number of adsorption sites constant so that on the clot surface $\frac{dc_s}{dt} = k_{ads}c$. Applying mass balance then results in the final boundary condition on the clot surface,

$$\vec{n} \cdot \left(c\vec{u} - \frac{1}{Pe} \nabla c \right) = Dam \cdot c \quad (4)$$

with $Dam = \frac{k_{ads}}{U_\infty}$ the Damköhler number.

Simulations were performed with COMSOL 5.6a, and further details on numerical implementation and a mesh convergence study are reported in the Supporting Information.

3 Results

This section presents the findings of a systematic numerical analysis focusing on reactivity, hemodynamics, and permeability. The results have been evaluated for the following range of parameters: Reynolds number ($1 \leq Re \leq 100$); Darcy number ($10^{-6} \leq Da \leq 10^{-3}$); Damköhler number of ($0 \leq Dam \leq 10^2$); and domain blockage ratio (β) with values 0.25 and 0.5. Further details are presented in Table 1.

3.1 Impact of clot permeability on hemodynamics

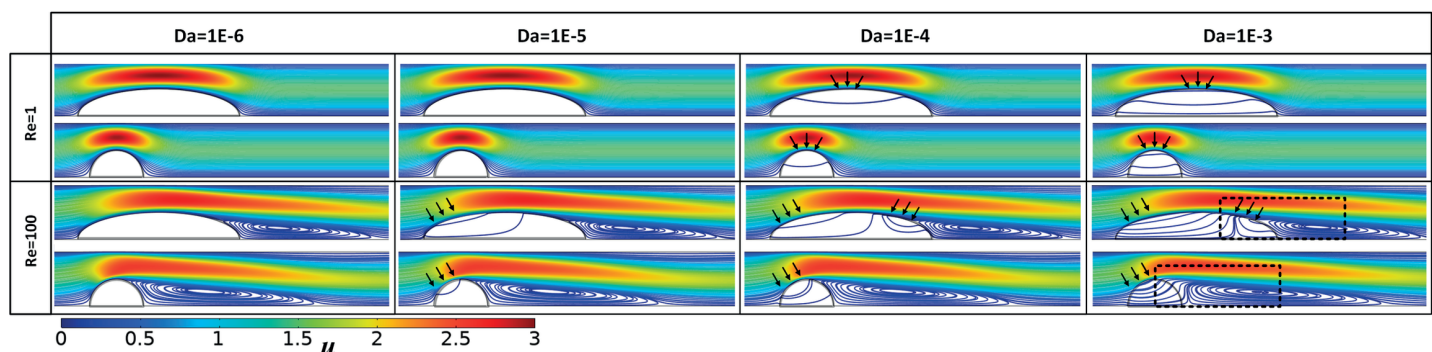
Flow lines and velocity magnitudes for the semi-circular and semi-elliptical permeable clots for $Re = 1, 100, \beta = 0.5$, and the full range of Darcy numbers is shown in Fig 2 and for $\beta = 0.25$ in Fig 3A. Results for additional Re numbers are shown in Fig S1.

For $Da \leq 10^{-5}$ and $Re \leq 1$ the clots behave like impermeable objects. Under low-flow conditions ($Re \leq 1$), increasing the Da to 10^{-3} results in partial flow through the center of the clot. In contrast, under high-flow conditions $Re > 50$, a distinct alteration in flow pattern becomes apparent. For $Da \leq 10^{-6}$ clots still behave as solid objects, but already for $Da = 10^{-5}$ blood flow initially moves through the upper layer of the clot (highlighted by black arrows in Fig 2). For $Da = 10^{-4}$, blood flow from both sides causes an impact on the semi-elliptical shape, whereas, for the circular shape, it solely affects the upstream side of the clot. For $Da \geq 10^{-4}$ the recirculating zone starts to separate from the clot shape and shifts downstream for the semi-circular

Table 1. Parameter used in simulations.

Notation	Definition	Value	Reference
Re	Reynolds number	1 to 100	Re values range from 0.01 [18] in small arteries to 334 for white clots growth in stenotic regions [36].
Da	Darcy number	10^{-6} to 10^{-3}	A wide range of reported clot permeabilities [34] $(2.6 \pm 1.2) \times 10^0 (\mu\text{m}^2)$ to $(1.5 \pm 0.3) \times 10^{-5} (\mu\text{m}^2)$ height of the domains (30 μm to 3 mm) and varying blockage ratios.
Dam	Damköhler number	0 to 10^2	An enhanced adhesion rate is defined as [46]: $k_i(x) = k_{ads} \cdot (1 + \lambda \cdot \dot{\gamma}_w(x))$ where $\dot{\gamma}_w(x)$ is the local wall shear rate, λ is the shear enhancement factor, k_{ads} of $[10^{-3}, 10^{-4}, 10^{-5}] \text{ ms}^{-1}$ [39]. Varying flow inlet velocities: stenotic conditions, capillary tubes, etc.
Pe	Peclet number	10^5	A constant value of domain Peclet number is used (platelet diffusivity (D) is $1.57 \times 10^{-5} \text{ mm}^2 \text{ s}^{-1}$ [40]), the Peclet-Damköhler interplay is reported by [17].
U_∞	Average inlet velocity	1	-
c_0	Inlet concentration	1	-
h	Clot height	1	Dimensionless experiment set-up.
H	Domain height	$\frac{h}{\beta}$	Dimensionless experiment set-up with $\beta = 0.25, 0.5$
L	Domain length	$16h$	Dimensionless experiment set-up.
-	Boundary element size	$0.01h$	-

<https://doi.org/10.1371/journal.pone.0317828.t001>

**Fig 2. Flow streamlines and velocity magnitudes over varying ranges of Darcy numbers for semi-circular and semi-elliptical, permeable clots ($\beta = 0.5$).**

<https://doi.org/10.1371/journal.pone.0317828.g002>

clot, while for the semi-elliptical clot, the recirculating zone moves upstream and into the permeable clot. By increasing the permeability of the clot, similar flow characteristics can be achieved at higher clot heights under comparable flow conditions. For instance, a semi-elliptical configuration with a β value of 0.25 induces a flow streamline similar to one with a β value of 0.5 with a Darcy number by one magnitude unit higher (as shown in Fig 3A). Moreover, this observation emphasizes the reduced impact of lower clot permeability on the flow behavior surrounding permeable clots in lower vessel blockage ratios. With the β value of 0.25, the solid behavior of a clot with a Darcy number of 10^{-5} is sustained at a Reynolds number of up to 100.

In Fig 3B, two limiting scenarios are selected to show how platelet concentrations vary in a semi-elliptical clot. At a Dam value of 0, circulating platelets surrounding the clot interface do not react, and their concentration pattern is defined only through the processes of advection and diffusion. As a result, platelets accumulate on the upstream side of the clot due to the positive normal velocity (where a positive velocity means flow toward the surface)

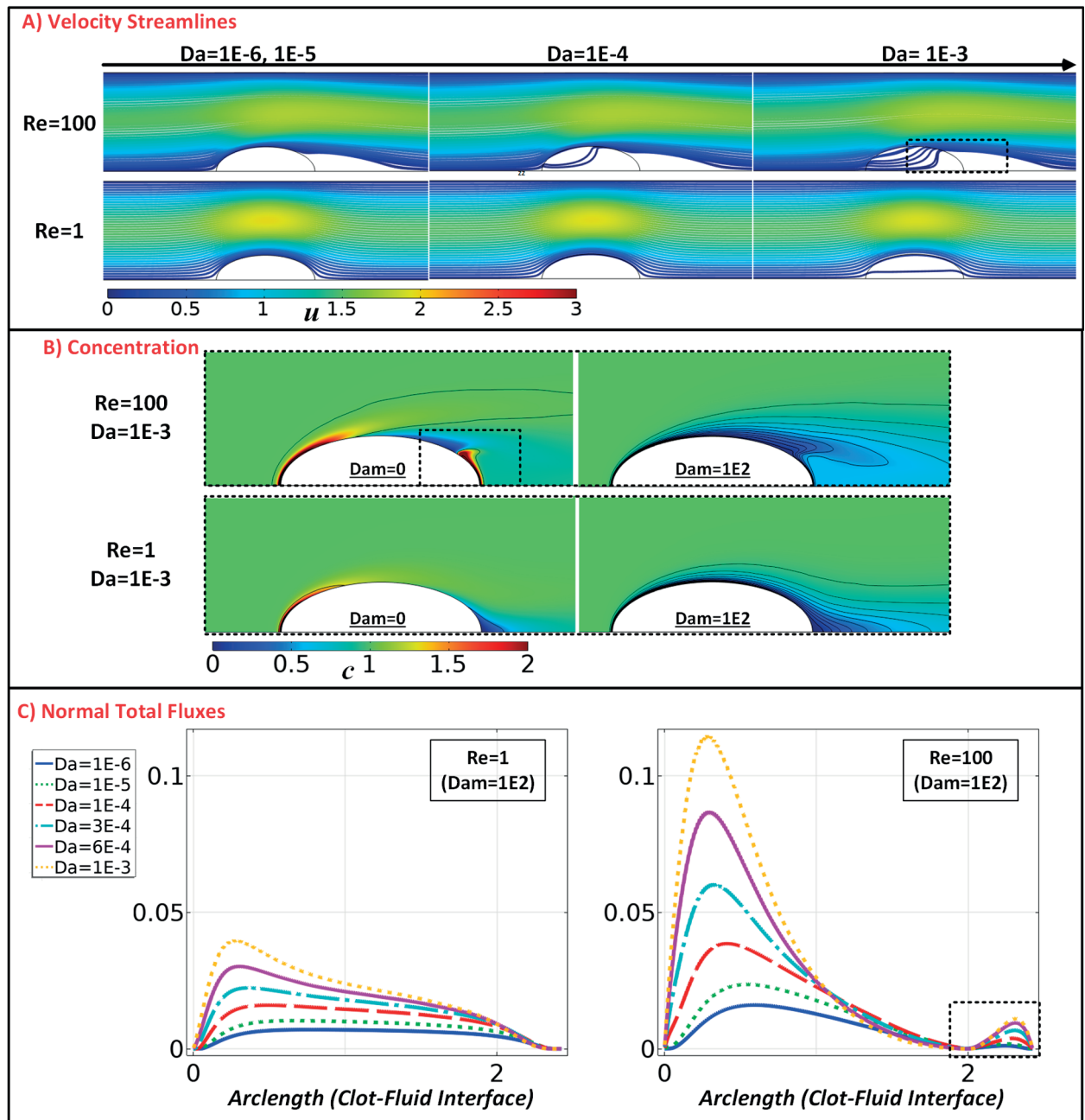


Fig 3. Representation of (A) flow streamlines and velocity magnitude, (B) concentration of platelets, and (C) distribution of the normal total flux to clot interface in a semi-elliptical clot with a blockage ratio of 0.25.

<https://doi.org/10.1371/journal.pone.0317828.g003>

along the clot interface. In comparison, the negative normal velocity at the downstream side causes platelets to be washed away except in the area with overlapping wake zones. Specifically, this phenomenon leads to a positive accumulation of platelets and positive normal total fluxes behind permeable semi-elliptical clots (as shown with dashed lines, Fig 3B). In the second scenario, increased platelet reactivity accelerates the free-flowing platelets' bonding process to the boundary layer. This substantially reduces the availability of platelets surrounding the clot boundary layer, creating a concentration gradient near the clot (see Figs. 3B and

S4). Figure 3C shows the total platelet flux on the clot surface for the semi-elliptical case with a blockage ratio $\beta = 0.25$, $Dam = 10^2$, and $Re = 1$ and 100. An increase in clot permeability leads to a proportionate increase in total platelet flux under both low and high-flow conditions, with the largely unaffected normal total flux pattern over the clot interface, especially for low-flow conditions (see Supporting Information for other parameter settings, leading to comparable observations). This suggests higher clot growth rates for more significant clot permeability, while the shape of the growing clot is not very much influenced by the permeability. Increasing Da from 10^{-6} to 10^{-3} for both $Re = 1$ and 100 resulted in an approximately four-fold increase in the maximum total platelet flux. At a Reynolds number of 100, the graph depicts an abrupt rise in overall flux over the first half of the clot for high permeabilities, followed by a notable decrease in the second half. The phenomenon can increase the growth rate under high-flow conditions (Fig 3C) by amplifying the adhesion of platelets at the upstream side of permeable clots.

3.2 Impact of clot permeability and binding kinetics on platelet fluxes at the clot surface

Figure 4A shows normal flow velocities over the clot surface for semi-circular clots (The horizontal axis represents the arc length of the clot interface) for the full range of Darcy numbers. At small Das , the normal velocities are very close to zero, and for $Da \geq 10^{-4}$, substantial normal flows, primarily positive at the upstream face and negative at the downstream face, can be observed. During the assessment of the normal flow characteristics, the permeable clot exhibits a symmetrical distribution of positive and negative flow velocities along the y -axis, with a Reynolds number of 1 and the Darcy number of 10^{-3} (Fig 4A). At a Reynolds number of 100, an asymmetrical velocity pattern emerges, suggesting the existence of a recirculation region in the clot downstream (as shown in Fig 4B by the black arrow). Figure 4B shows platelet concentrations for semi-circular clots in two scenarios. In the absence of binding reactivity, the high-flow rate (large Pe) leads to significantly more platelet accumulation at the upstream face of the clot (see black arrow in Fig 4B). For $Re = 100$, the wake structure primarily limits the availability of platelets to this region (see black arrow in Fig 4B). Mainly, for $Dam = 0$, there is an accumulation and depletion of platelets over a more extensive area surrounding the clot interface, while for $Re = 1$, this impact is primarily restricted to the close vicinity of the interface. Note that for the semi-elliptical cases, both blockage ratios (see S2 Fig) display a positive normal velocity at the upstream of the clot when the wake structure shifts upward for $Da \geq 10^{-4}$ leading to a continuous build-up of platelets within this region. For $Dam = 10^2$, most platelets arriving at the clot surface are removed from the fluid and bounded to the clot surface, rendering the concentration of free-flowing platelets in the fluid at the clot surface nearly zero. Note that this can lead to strong concentration gradients at the surface, hence strong normal positive diffusive fluxes towards the surface (see, e.g., Figs. 6 and S3). A normal total flux pattern similar to semi-elliptical cases is observed over varying ranges of Darcy numbers, except for the absence of normal total flux accumulation downstream of the clots (Fig 4C).

The total normal flux of platelets on the clot surface (The horizontal axis represents the arc length of the clot interface) consists of a normal diffusive and advective part. Figure 5 shows those fluxes for a semi-elliptical clot with a blockage ratio $\beta = 0.5$, negligible reactivity $Dam = 10^{-4}$, and a range of Da numbers. Regardless of flow conditions, the normal diffusive flux counteracts the normal advective flux across all Darcy numbers, resulting in an almost negligible total flux. A positive normal advective flux is observed at the downstream side of the clot

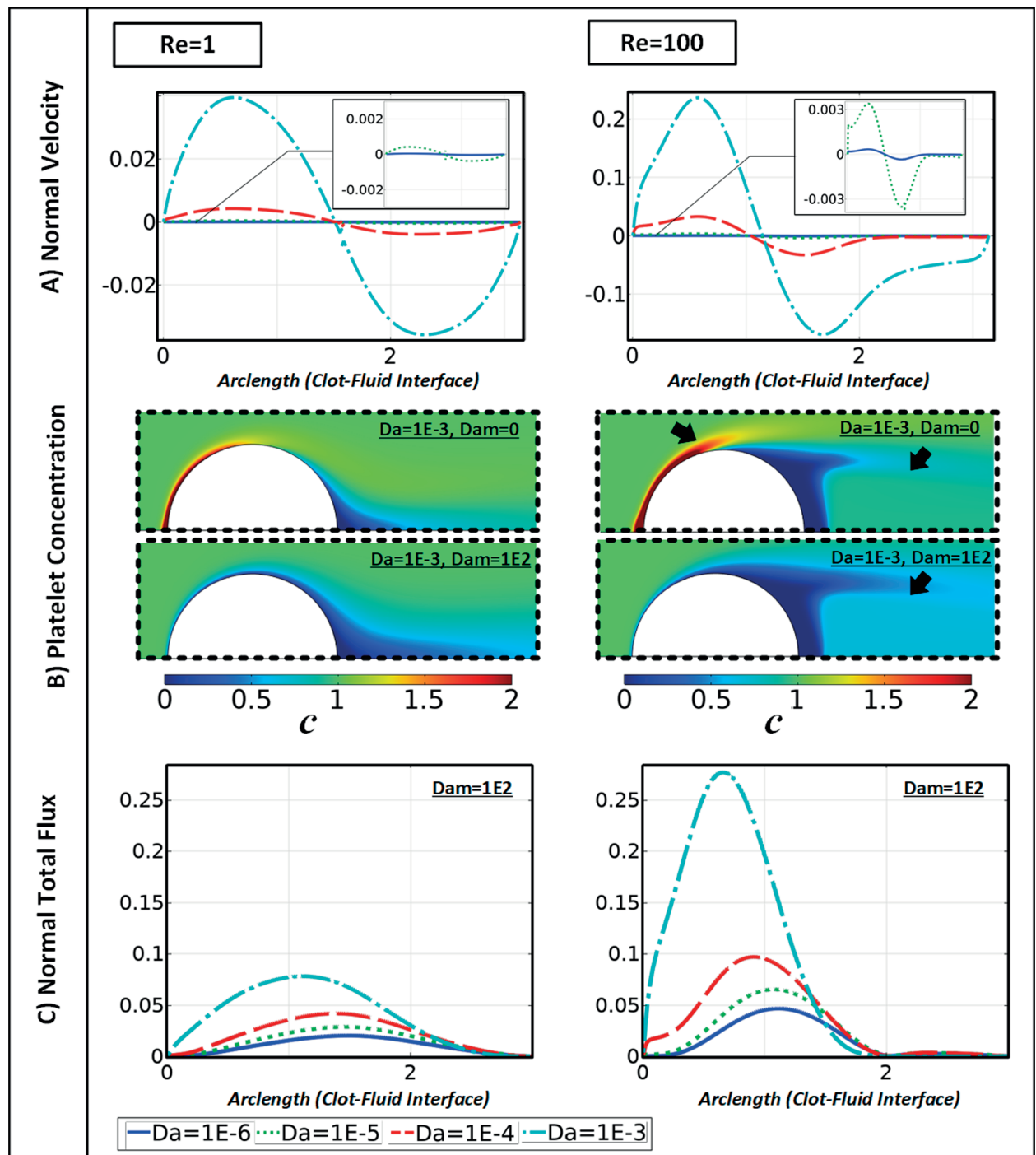


Fig 4. (A) Normal velocity distribution across the clot interface for a varying range of Darcy numbers, and (B) concentration of platelets, and (C) distribution of the normal total flux to clot interface in a semi-circular clot with a blockage ratio of 0.5.

<https://doi.org/10.1371/journal.pone.0317828.g004>

interface due to the overlapping of the circulating zone with the clot structure. Subsequently, this leads to a negative normal diffusive flux, promoting the accumulation of platelets in this area.

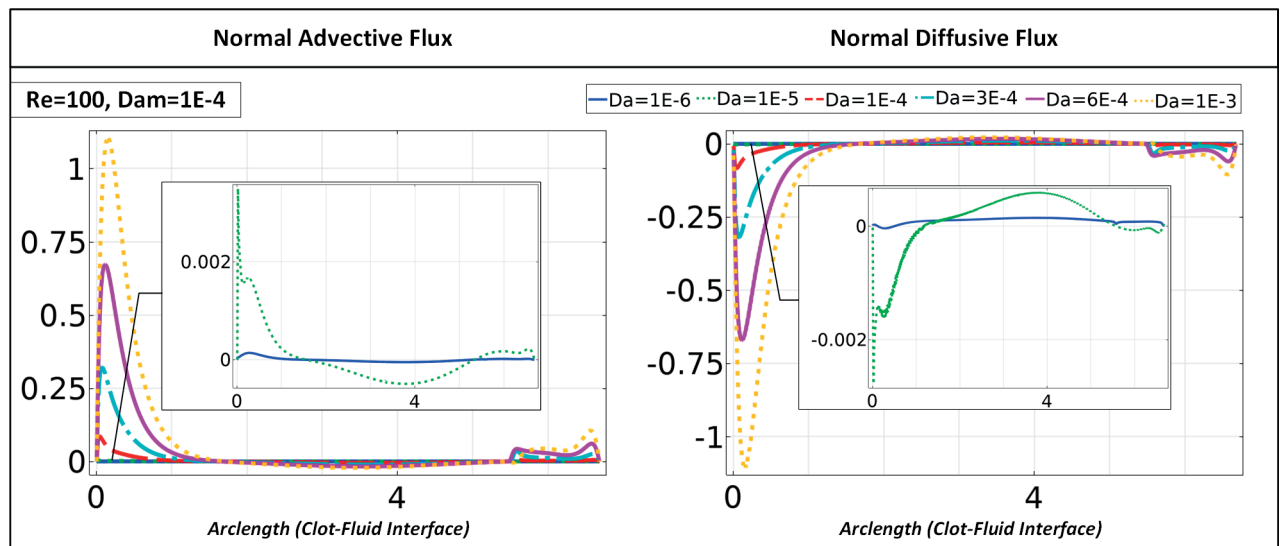


Fig 5. A comparison of the normal advective and normal diffusive flux at the clot-fluid interface is shown for a semi-elliptical clot with a blockage ratio of 0.5.

<https://doi.org/10.1371/journal.pone.0317828.g005>

Finally, mean values of normal advective, diffusive, and total flux, averaged over the clot surface, are shown in Figs. 6, 7, and S3. The mean fluxes are calculated to interpret the underlying physics, particularly in relation to clot growth behavior across varying permeability ranges. Regardless of clot permeability, $Dam \leq 10^{-3}$ results in a positive concentration gradient, causing the abundance of circulating platelets near the clot interface. Accordingly, both clot shapes demonstrate a balance between the normal advective and diffusive fluxes within this reactivity range, resulting in close to zero normal total flux. With Damköhler values reaching 10^{-2} , the dynamic behavior of platelets counters a transition pattern governed by clot permeability. Except for Re of 1 in semi-elliptical case, with such reactivity in both flow conditions, an increase of Darcy number higher than 10^{-4} suppresses the impact of clot reactivity and leads to platelet accumulation at the clot interface (positive gradient of concentration). The transition in platelet distribution due to variations in clot permeability can be observed, for example in low-flow conditions for a semi-elliptical clot shape $\beta = 0.5$, beginning at a Damköhler number Dam of 10^{-3} and Da of 10^{-4} . Lastly, as the Dam increases, a higher clot permeability is required to introduce an accumulation of platelets in the boundary layer.

During the assessment of the normal velocity arising around semi-circular clots, it was observed that the clot interface experiences a maximum normal velocity that is up to twice as high as that of semi-elliptical clots, given similar flow conditions and Darcy numbers (as depicted in Figs. 3B and S2). This phenomenon can be attributed to the higher interface curvature of the semi-circular clot shape, which causes more significant flow blockage in the vessel. In contrast, the semi-elliptical shape facilitates the partial passage of tangential flow over the interface, resulting in a decrease in normal velocity and, subsequently, a significant reduction in advective flux. This can explain why the increasing clot Darcy number, even in low-flow conditions in the semi-circular case, could cause a more predominant effect concerning clot reactivity. Regardless of clot permeability, flow condition, or shape, when the Damköhler number Dam reaches or exceeds 10^{-2} , the clot interface begins to experience a reduction in circulating platelets at the reactive boundary layer. This shortage in platelet availability may

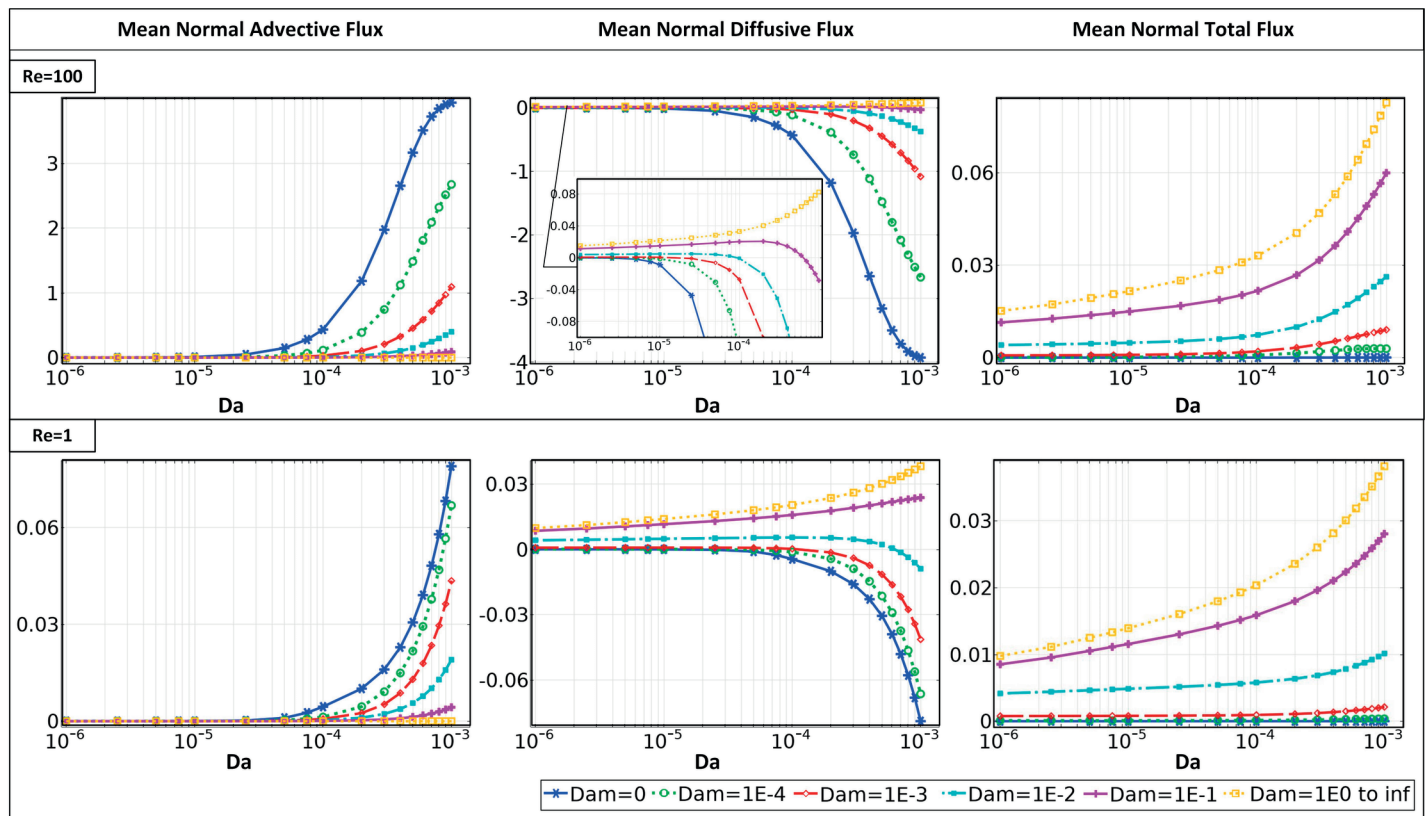


Fig 6. The mean normal advective and mean normal diffusive, and mean normal advective flux across the interface of a semi-circular clot with $\beta = 0.5$ for different Da and Dam ranges, at $Re = 100$ and $Re = 1$.

<https://doi.org/10.1371/journal.pone.0317828.g006>

start to limit further growth, as the initial flux increase transitions into a regulated, steady growth rate.

Under high-flow rate conditions, the semi-circular shape exhibits up to twice the maximum total flow and experiences up to 30 percent higher platelet total normal flux in low-flow conditions compared to semi-elliptical clots. Consistent with expectations, increasing the blockage ratio yields a greater total flux at the clot interface (see Figs. S3 and 7). The results displayed in Figs. 6 and 7 demonstrate a significant increase in the total flux, up to four times, as the clot permeability rises from a Da value of 10^{-6} to 10^{-3} . The maximum alteration is seen in the highest reactivity condition with a Dam of 100.

4 Discussion

Research focused on computational models and experiments related to clot formation in arteries and veins has contributed valuable insights into the composition and structure of blood clots [53,54]. Notably, the timing, composition, and structure of a blood clot can be influenced by different methods of inducing thrombosis. The existence of various pathological environments underscores the importance of comprehending platelet transport characteristics for clot formation. Here, a novel computational framework is developed to analyze how influential metrics are related to platelet behavior, blood flow, and flow-mediated transport near a clot region. Particularly, the clot boundary layer experiences a specific pressure gradient due to different flow conditions and permeability, which, combined with binding kinetics,

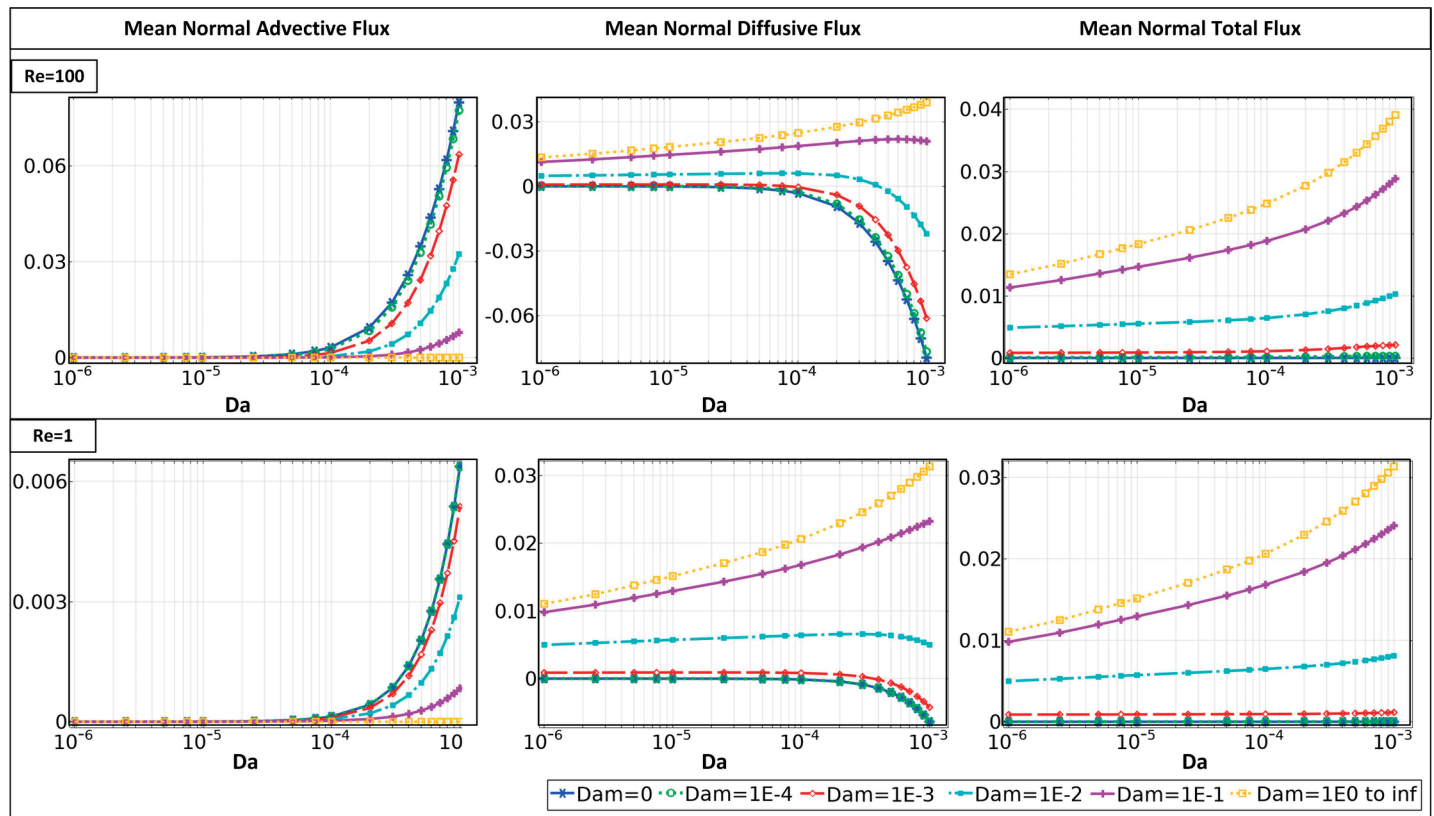


Fig 7. The mean normal advective, mean normal diffusive, and mean normal total flux across the interface of a semi-elliptical clot with $\beta = 0.5$ for different Da and Dam ranges, at $Re = 100$ and $Re = 1$.

<https://doi.org/10.1371/journal.pone.0317828.g007>

can influence platelet transport behavior. In related research, Teeraratkul et al. [55] examined how different factors, such as thrombus shape, microstructure, and degree of wall damage, impact hemodynamic characteristics and the local rotational region within the thrombus neighborhood. The study showed that leakage caused by the damaged wall can alter the pressure gradient of the boundary and significantly affect the interplay of advection and diffusion that governs flow-mediated transport. Furthermore, they highlight that the presence of small interstitial spaces in the microstructure establishes a transport regime that favors dominant diffusion and a low Peclet number. In an earlier study, Tomaiuolo et al. [18] revealed that the microenvironment within the thrombus is primarily diffusion-dominated due to the small pore size. Even when the lumen velocity was increased four times to reach 8 mm/s, the average clot velocity remained significantly lower than the bulk velocity. The researchers concluded that the presence and location of a tightly packed thrombus core had minimal effect on the flow velocity within the mass.

It is worth noting that previous studies have mainly focused on the characteristics outside or within clots that are tightly packed (low porosity) and under low flow conditions (Re less than 1), which reduces the impact of pressure gradient on transport characteristics. Meanwhile, at low Reynolds number and low permeability, our flow pattern result is consistent (see Fig 2) with these findings. However, recent research [36] has shown that the pores observed in the transverse clot section confirm the high permeability of the SIPA clot. The high permeability of this internal clot [11] facilitates effective drug transportation through

flow movement within the clot's domain. Our computational framework enabled the precise depiction of the diverse flow pattern observed in varying flow conditions, as well as the enhanced or hindered transport of platelets towards the permeable layer.

The visualization of flow streamlines in the $Re \leq 50$ and $Da \leq 10^{-3}$ regime demonstrates (see Figs. 2 and S1) that changes in clot permeability have a negligible impact on the flow profile, highlighting the essential role of diffusion in the flow-mediated transport mechanism under these circumstances. In the rest of the conditions, the clot mainly permits partial fluid flow, limiting the fluid streamlines' reach to the attachment region of the clots. Regarding species transport in this regime, the core part of the clot remains unaffected by the advection of agonists. In agreement with earlier studies [18,55], our results indicate that as the Reynolds number decreases, the flow structure has little influence on the inner structure of the clot, especially for low permeabilities (as shown in Figs. 2 and S1). This creates a hemodynamic condition that favors diffusion [32]. It is shown that although the Darcy number has minimal impact on the streamline at low Re (1 or lower), there is a significant difference at high Re (greater than 50), highlighting the role of advection in the flow-mediated transport mechanism. This can directly influence platelets' effective concentration and distribution pattern (as shown in Fig 3) and soluble agonists inside and outside growing clots at pathological high shear rates. Furthermore, we have shown that the normal flow velocity towards the clot interface and circulating zone behind the clot structure [56] regulate the concentration profile of free-flowing platelets, which could explain both the pattern and magnitude of the total normal flux in this region (as seen in Fig 4).

Here, the importance of implementing a semipermeable membrane boundary condition, which restricts platelet movement within the clot while allowing plasma flow is highlighted. This leads to two primary mechanisms that regulate the diffusion of platelets and concentration gradients at the clot boundary layer: surface reactions and the advection of platelets to the interface. It was observed that once the Darcy number surpasses 10^{-3} , the increased permeability permits a more significant fluid influx towards the clot, resulting in a significantly higher normal total flux. Nonetheless, the platelet availability pattern derived from the normal fluxes remained largely unaffected by the increase in the Darcy number. In particular, the first half of the clot is mainly an abundance of platelets, while the clot shape determines how the wake structure behind the clot regulates platelet transport in this region. A recent study [57] indicates that the movement of platelets surrounding thrombi is influenced by the interplay between the viscoelastic forces produced by interplatelet bonds and fluid drag. They revealed that the formation of stable occlusive thrombi is contingent upon specific combinations of model parameters, including rates and the number of bonds necessary for platelet attachment. Clotting can be initiated by different mechanisms, including contact-induced activation, platelet activation due to shear rate, and interactions between platelets and red blood cells. Particularly in relatively slow flows within stagnation and recirculation zones, the activation by platelet-platelet and red blood cell (RBC)-platelet interactions becomes noteworthy. The study by Bouchnita et al. [58] underscores the significant role of recirculation zones in the stagnation of RBCs, influencing the spatial propagation and temporal dynamics of aneurysmal thrombus growth.

Carminita et al. [59] demonstrated that thrombus growth is influenced by the spatial distribution of platelets, exhibiting a transverse activation gradient from the injured endothelium towards the vessel's periphery. According to the studies, it was determined that a thrombus consists of three distinct platelet sub-populations, resulting in a dual gradient in both the transversal and longitudinal axis of the thrombus. The highest concentration of fully activated platelets was observed in close proximity to the injury site. Our findings have demonstrated that the combined effect of the specific value range of clot permeability, flow rate, and

clot shape can intensify the platelet flux at the upstream side of the clot. In a study by Rana et al. [60], it has been demonstrated that a specific geometry of an obstructed blood vessel, accompanied by a high local flow rate and subsequent spatial micro shear gradient, induces the formation of a spatial pattern of thrombus due to increased activity of vWF. In conclusion, this investigation examines how hemodynamics, clot permeability, and binding kinetics collectively impact the platelet's transport [62,63] processes near a permeable boundary layer. Highlighting that the derived interplay between the pressure gradient and reaction rate in this boundary can hinder or expedite the movement of platelets within this layer. This research underscores the importance of accurately estimating the permeability of blood clots in different flow conditions in order to predict the initiation and development of thrombus.

5 Limitation

This benchmark only considers a two-dimensional setup. Key findings are expected to have similar applicability in a three-dimensional setting. In our analysis, the impact of shear-dependent binding kinetics caused by vWF and the influence of chemical-induced binding kinetics influenced by species, such as ADP were neglected, as well as the shear-induced margination of platelets. Incorporating platelet activation as a dynamic, shear-dependent variable would strengthen the model by accounting for activation thresholds, agonist availability, and local hemodynamic variations, providing a more accurate representation of thrombus development. Future model extensions could integrate variable activation states with spatial gradients and responses to shear changes, enhancing physiological relevance and advancing our understanding of thrombus initiation and growth across diverse vascular environments. In this model, a steady rather than pulsatile blood flow is assumed to simplify hemodynamic representation. However, in physiological conditions, blood flow is inherently pulsatile, particularly in arteries where pressure and flow fluctuate with each cardiac cycle. These pulsatile dynamics can influence platelet transport, adhesion, and clot growth in important ways. For example, periodic high-velocity peaks in pulsatile flow may enhance platelet transport toward the clot by intermittently increasing advective flux, thereby potentially boosting platelet deposition rates at the clot interface. Furthermore, variations in shear stress from pulsatile flow may affect platelet activation, as mechanisms such as von Willebrand factor-mediated adhesion are highly responsive to changes in shear rate. This periodic shear could create more complex adhesion and detachment behaviors than a steady-state model can accurately represent. Future studies could incorporate pulsatile flow components to better simulate oscillatory shear forces and their effects on platelet behavior, thereby enhancing the physiological accuracy of the model for applications in arterial thrombus formation. The impact of tangential platelet flux on the clot surface was not considered. Authors in [26,61] state that tangential platelet flux is also observed as a source of platelet cohesion and adhesion in the growing clot. The heterogeneity of the clot, e.g., in terms of a dense core and a more permeable shell, was also not considered. However, according to Tomaiuolo et al. [18], the transport mechanism at the clot shell zone is not significantly affected by the location and composition of the core. Integrating a heterogeneous clot structure may influence the observed internal flow pattern in high-flow conditions. The stationary geometry assumption might have limited validity for dynamic growth circumstances given the considerable impact of growing thrombi on flow patterns, flow rate, and platelet transport kinetics [46].

6 Conclusion

Our study employs a systematic numerical analysis of flow characteristics, platelet distribution, and transfer in a 2D rectangular domain featuring semi-circular and semi-elliptical

clots under steady-state conditions as a function of clot permeability and binding reaction rates. The results show that permeability significantly influences flow patterns inside and in the vicinity of the clot in high-flow conditions, particularly for $Re \geq 50$. Specifically, semi-circular clots subjected to high-flow rates ($Re=100$) experience up to twice the normal total flux of platelets compared to semi-elliptical clots. This study illustrates how distinctive blood flow velocity patterns, symmetrical and asymmetrical (given the circulating zone behind the clots), across a varying range of clot permeability, dictate platelets' availability and mass transfer behavior over the clot interface. Moreover, under low- and high-flow conditions, total platelet flux toward the clot for high permeable clots can be up to four times that of an impermeable clot. In the following study, we will further investigate the contribution of clot permeability and binding kinetics in the platelet static and dynamic behavior during permeable clot growth.

Supporting information

S1 Text. Numerical implementation and validation. This file includes detailed descriptions of the grid convergence study, numerical implementation, and validation results [51].

Author contributions

Conceptualization: Niksa Mohammadi Bagheri, Alfons G. Hoekstra.

Formal analysis: Niksa Mohammadi Bagheri.

Funding acquisition: Gabor Závodszy, Alfons G. Hoekstra.

Methodology: Niksa Mohammadi Bagheri.

Supervision: Gabor Závodszy, Alfons G. Hoekstra.

Validation: Niksa Mohammadi Bagheri.

Writing – original draft: Niksa Mohammadi Bagheri.

Writing – review & editing: Niksa Mohammadi Bagheri, Gabor Závodszy, Alfons G. Hoekstra.

References

1. Gutiérrez NG, Shankar KN, Sinno T, Diamond SL. Thrombosis and hemodynamics: External and intrathrombus gradients. *Curr Opin Biomed Eng.* 2021;19:100316. <https://doi.org/10.1016/j.cobme.2021.100316> PMID: 34693101
2. Belyaev AV, Dunster JL, Gibbins JM, Pantelev MA, Volpert V. Advancing research on blood coagulation and thrombosis: Reply to the comments on "Modeling thrombosis in silico: Frontiers, challenges, unresolved problems and milestones". *Phys Life Rev.* 2018;26-27:116–9. <https://doi.org/10.1016/j.plrev.2018.09.006> PMID: 30297158
3. Nesbitt WS, Westein E, Tovar-Lopez FJ, Tolouei E, Mitchell A, Fu J, et al. A shear gradient-dependent platelet aggregation mechanism drives thrombus formation. *Nat Med.* 2009;15(6):665–73. <https://doi.org/10.1038/nm.1955> PMID: 19465929
4. Van Rooij BJ, Závodszy G, Hoekstra AG, Ku DN. Biorheology of occlusive thrombi formation under high shear: In vitro growth and shrinkage. *Sci Rep.* 2020;10(1):18604. <https://doi.org/10.1038/s41598-020-74518-7> PMID: 33122712
5. Diamond SL. Systems biology of coagulation. *J Thromb Haemost.* 2013;11(Suppl. 1):224–32. <https://doi.org/10.1111/jth.12220> PMID: 23809126
6. Van Rooij BJM, Závodszy G, Azizi Tarksalooyeh VW, Hoekstra AG. Identifying the start of a platelet aggregate by the shear rate and the cell-depleted layer. *J R Soc Interface.* 2019;16(159):20190148. <https://doi.org/10.1098/rsif.2019.0148> PMID: 31575344

7. Liu ZL, Bresette C, Aidun CK, Ku DN. SIPA in 10 milliseconds: VWF tentacles agglomerate and capture platelets under high shear. *Blood Adv*. 2022;6(8):2453–65. <https://doi.org/10.1182/bloodadvances.2021005692> PMID: 34933342
8. Casa LDC, Ku DN. Thrombus formation at high shear rates. *Annu Rev Biomed Eng*. 2017;19(April):415–33. <https://doi.org/10.1146/annurev-bioeng-071516-044539> PMID: 28441034
9. Taylor JO, Witmer KP, Neuberger T, Craven BA, Meyer RS, Deutsch S, et al. In vitro quantification of time dependent thrombus size using magnetic resonance imaging and computational simulations of thrombus surface shear stresses. *J Biomech Eng*. 2014;136(7):1.4027613. <https://doi.org/10.1115/1.4027613> PMID: 24805351
10. Menichini C, Cheng Z, Gibbs RGJ, Xu XY. Predicting false lumen thrombosis in patient-specific models of aortic dissection. *J R Soc Interface*. 2016;13(124):20160759. <https://doi.org/10.1098/rsif.2016.0759> PMID: 27807275
11. Du J, Kim D, Alhawael G, Ku DN, Fogelson AL. Clot permeability, agonist transport, and platelet binding kinetics in arterial thrombosis. *Biophys J*. 2020;119(10):2102–15. <https://doi.org/10.1016/j.bpj.2020.08.041> PMID: 33147477
12. Tovar-Lopez FJ, Rosengarten G, Westein E, Khoshmanesh K, Jackson SP, Mitchell A, et al. A microfluidics device to monitor platelet aggregation dynamics in response to strain rate micro-gradients in flowing blood. *Lab Chip*. 2010;10(3):291–302. <https://doi.org/10.1039/b916757a> PMID: 20091000
13. Yang L, Neuberger T, Manning KB. In vitro real-time magnetic resonance imaging for quantification of thrombosis. *MAGMA*. 2021;34(2):285–95. <https://doi.org/10.1007/s10334-020-00872-2> PMID: 32729094
14. Wootton DM, Ku DN. Fluid mechanics of vascular systems, diseases, and thrombosis. *Annu Rev Biomed Eng*. 1999;1:299–329. <https://doi.org/10.1146/annurev.bioeng.1.1.299>
15. Brass LF, Diamond SL. Transport physics and biorheology in the setting of hemostasis and thrombosis. *J Thromb Haemost*. 2016;14(5):906–17. <https://doi.org/10.1111/jth.13280> PMID: 26848552
16. Preissner KT. Biochemistry and physiology of blood coagulation and fibrinolysis. *Hamostaseologie*. 2004;24(2):84–93. <https://doi.org/10.1267/hamo04020084> PMID: 15136873
17. Rana K, Neeves KB. Blood flow and mass transfer regulation of coagulation. *Blood Rev*. 2016;30(5):357–68. <https://doi.org/10.1016/j.blre.2016.04.004> PMID: 27133256
18. Tomaiuolo M, Stalker TJ, Welsh JD, Diamond SL, Sinno T, Brass LF. A systems approach to hemostasis: 2. Computational analysis of molecular transport in the thrombus microenvironment. *Blood*. 2014;124(11):1816–23. <https://doi.org/10.1182/blood-2014-01-550343> PMID: 24951425
19. Tokarev AA, Butylin AA, Ataulakhanov FI. Platelet adhesion from shear blood flow is controlled by near-wall rebounding collisions with erythrocytes. *Biophys J*. 2011;100(4):799–808. <https://doi.org/10.1016/j.bpj.2010.12.3740> PMID: 21320422
20. Kaneva VN, Dunster JL, Volpert V, Ataullahanov F, Pantelev MA, Nechipurenko DY. Modeling thrombus shell: Linking adhesion receptor properties and macroscopic dynamics. *Biophys J*. 2021;120(2):334–51. <https://doi.org/10.1016/j.bpj.2020.10.049> PMID: 33472026
21. Leiderman K, Fogelson AL. The influence of hindered transport on the development of platelet thrombi under flow. *Bull Math Biol*. 2013;75(8):1255–83. <https://doi.org/10.1007/s11538-012-9784-3> PMID: 23097125
22. Stalker TJ, Traxler EA, Wu J, Wannemacher KM, Cermignano SL, Voronov R, et al. Hierarchical organization in the hemostatic response and its relationship to the platelet-signaling network. *Blood*. 2013;121(10):1875–85. <https://doi.org/10.1182/blood-2012-09-457739> PMID: 23303817
23. Voronov RS, Stalker TJ, Brass LF, Diamond SL. Simulation of intrathrombus fluid and solute transport using in vivo clot structures with single platelet resolution. *Ann Biomed Eng*. 2013;41(6):1297–307. <https://doi.org/10.1007/s10439-013-0764-z> PMID: 23423707
24. Ghezelbash F, Liu S, Shirazi-Adl A, Li J. Blood clot behaves as a poro-visco-elastic material. *J Mech Behav Biomed Mater*. 2022;128:105101. <https://doi.org/10.1016/j.jmbbm.2022.105101> PMID: 35124354.
25. Xu S, Xu Z, Kim OV, Litvinov RI, Weisel JW, Alber M. Model predictions of deformation, embolization and permeability of partially obstructive blood clots under variable shear flow. *J R Soc Interface*. 2017;14(136):20170441. <https://doi.org/10.1098/rsif.2017.0441> PMID: 29142014.
26. Leiderman K, Fogelson AL. Grow with the flow: A spatial-temporal model of platelet deposition and blood coagulation under flow. *Math Med Biol*. 2011;28(1):47–84. <https://doi.org/10.1093/imammb/dqq005> PMID: 20439306
27. Chernysh IN, Nagaswami C, Kosolapova S, Peshkova AD, Cuker A, Cines DB, et al. The distinctive structure and composition of arterial and venous thrombi and pulmonary emboli. *Sci Rep*. 2020;10(1):5112. <https://doi.org/10.1038/s41598-020-59526-x> PMID: 32198356

28. Wufsus AR, MacEra NE, Neeves KB. The hydraulic permeability of blood clots as a function of fibrin and platelet density. *Biophys J*. 2013;104(8):1812–23. <https://doi.org/10.1016/j.bpj.2013.02.055> PMID: 23601328
29. Wufsus AR, Neeves KB. Fluid and solute transport in the interstitial space of blood clots. In: Poate JM, Kazemi H, Illangasekare T (eds) *Pore Scale Phenomena: Frontiers in Energy and Environment*. World Scientific Series in Nanoscience and Nanotechnology, 10. World Scientific Pub Co. Inc. 2015; p. 457–73.
30. Kim OV, Xu Z, Rosen ED, Alber MS. Fibrin networks regulate protein transport during thrombus development. *PLoS Comput Biol*. 2013;9(6):e1003095. <https://doi.org/10.1371/journal.pcbi.1003095> PMID: 23785270
31. Muthard RW, Diamond SL. Side view thrombosis microfluidic device with controllable wall shear rate and transthrum pressure gradient. *Lab Chip*. 2013;13(10):1883–91. <https://doi.org/10.1039/c3lc41332b> PMID: 23549358
32. Hao Y, Závodszy G, Tersteeg C, Barzegari M, Hoekstra AG. Image-based flow simulation of platelet aggregates under different shear rates. *PLoS Comput Biol*. 2023;19(7):e1010965. <https://doi.org/10.1371/journal.pcbi.1010965> PMID: 37428797
33. Buerck JP, Foster KM, Larson PR, O'Rear EA. Shear stimulated red blood cell microparticles: Effect on clot structure, flow and fibrinolysis. *Biorheology*. 2023;59(1-2):43–59. <https://doi.org/10.3233/BIR-220012> PMID: 36970891
34. He D, Kim DA, Ku DN, Hu Y. Viscoporoelasticity of coagulation blood clots. *Extreme Mech Lett*. 2022;56:101859. <https://doi.org/10.1016/j.eml.2022.101859>
35. Petkantchin R, Rousseau A, Eker O, Boudjeltia KZ, Wertheimer P, Lyon HCD, et al. A simplified mesoscale 3D model for characterizing fibrinolysis under flow conditions. *Sci Rep*. 2023;13:13681. <https://doi.org/10.1038/s41598-023-40973-12023> PMID: 37608073
36. Kim DA, Ku DN. Structure of shear-induced platelet aggregated clot formed in an in vitro arterial thrombosis model. *Blood Adv*. 2022;6(9):2872–83. <https://doi.org/10.1182/bloodadvances.2021006248> PMID: 35086138
37. Muthard RW, Diamond SL. Blood clots are rapidly assembled hemodynamic sensors: Flow arrest triggers intraluminal thrombus contraction. *Arterioscler Thromb Vasc Biol*. 2012;32(12):2938–45. <https://doi.org/10.1161/ATVBAHA.112.300312> PMID: 23087356
38. Holme PA, Ørvim U, Hamers MJAG, Solum NO, Brosstad FR, Barstad RM, et al. Shear-induced platelet activation and platelet microparticle formation at blood flow conditions as in arteries with a severe stenosis. *Arterioscler Thromb Vasc Biol*. 1997;17(4):646–53. <https://doi.org/10.1161/01.atv.17.4.646> PMID: 9108776
39. Bark DL, Ku DN. Platelet transport rates and binding kinetics at high shear over a thrombus. *Biophys J*. 2013;105(2):502–11. <https://doi.org/10.1016/j.bpj.2013.05.049> PMID: 23870271
40. Sorensen EN, Burgreen GW, Wagner WR, Antaki JF. Computational simulation of platelet deposition and activation: I. Model development and properties. *Ann Biomed Eng*. 1999;27(4):436–48. <https://doi.org/10.1114/1.200> PMID: 10468228
41. Fogelson AL. Continuum models of platelet aggregation: Formulation and mechanical properties. *SIAM J Appl Math*. 1992;52(4):1089–110.
42. Taylor JO, Meyer RS, Deutsch S, Manning KB. Development of a computational model for macroscopic predictions of device-induced thrombosis. *Biomech Model Mechanobiol*. 2016;15(6):1713–31. <https://doi.org/10.1007/s10237-016-0793-2> PMID: 27169403
43. Wu WT, Jamiolkowski MA, Wagner WR, Aubry N, Massoudi M, Antaki JF. Multi-constituent simulation of thrombus deposition. *Sci Rep*. 2017;7:1–16. <https://doi.org/10.1038/srep42720> PMID: 28218279
44. DeCortin ME, Brass LF, Diamond SL. Core and shell platelets of a thrombus: A new microfluidic assay to study mechanics and biochemistry. *Res Pract Thromb Haemost*. 2020;4(7):1158–66. <https://doi.org/10.1002/rth2.12405> PMID: 33134782
45. Zhussupbekov M, Wu WT, Jamiolkowski MA, Massoudi M, Antaki JF. Influence of shear rate and surface chemistry on thrombus formation in micro-crevice. *J Biomech*. 2021;121:110397. <https://doi.org/10.1016/j.jbiomech.2021.110397> PMID: 33845357
46. Hosseinzadegan H, Tafti DK. A predictive model of thrombus growth in stenosed vessels with dynamic geometries. *J Med Biol Eng*. 2019;39(4):605–21. <https://doi.org/10.1007/s40846-018-0443-5>
47. Kuharsky AL, Fogelson AL. Surface-mediated control of blood coagulation: The role of binding site densities and platelet deposition. *Biophys J*. 2001;80(3):1050–74. [https://doi.org/10.1016/S0006-3495\(01\)76085-7](https://doi.org/10.1016/S0006-3495(01)76085-7) PMID: 11222273
48. Fogelson AL, Neeves KB. Fluid mechanics of blood clot formation. *Annu Rev Fluid Mech*. 2015;47:377–403. <https://doi.org/10.1146/annurev-fluid-010814-014513> PMID: 26236058

49. Mirramezani M, Herbig B, Stalker T, Netley L, Cooper M, Weisel J, et al. Platelet packing density is an independent regulator of the hemostatic response to injury. *J Thromb Haemost*. 2018;16(5):973–83. <https://doi.org/10.1111/jth.13986> PMID: 29488682
50. Rashidi S, Dehghan M, Ellahi R, Riaz M, Jamal-Abad MT. Study of stream wise transverse magnetic fluid flow with heat transfer around an obstacle embedded in a porous medium. *J Magn Magn Mater*. 2015;378:128–37. <https://doi.org/10.1016/j.jmmm.2014.11.020>
51. Yu P, Zeng Y, Lee TS, Chen XB, Low HT. Steady flow around and through a permeable circular cylinder. *Comput Fluids*. 2011;42(1):1–12. <https://doi.org/10.1016/j.compfluid.2010.09.040>
52. Kaur R, Chandra A, Sharma S. Momentum transfer across a semi-circular porous cylinder attached to a channel wall. *Meccanica*. 2021;56(9):2219–41. <https://doi.org/10.1007/s11012-021-01369-5>
53. Van Rooij BJM, Závodszy G, Hoekstra AG, Ku DN. Haemodynamic flow conditions at the initiation of high-shear platelet aggregation: A combined in vitro and cellular in silico study. *Interface Focus*. 2021;11(1):20190126. <https://doi.org/10.1098/rsfs.2019.0126> PMID: 33335707
54. Spieker CJ, Závodszy G, Mouriaux C, Mangin PH, Hoekstra AG. Initial platelet aggregation in the complex shear environment of a punctured vessel model. *Phys Fluids*. 2023;35(7).
55. Teeraratkul C, Irwin Z, Shadden SC, Mukherjee D. Computational investigation of blood flow and flow-mediated transport in arterial thrombus neighborhood. *Biomech Model Mechanobiol*. 2021;20(2):701–15. <https://doi.org/10.1007/s10237-020-01411-7> PMID: 33438148
56. Tovar-Lopez FJ, Rosengarten G, Nasabi M, Sivan V, Khoshmanesh K, Jackson SP, Mitchell A, Nesbitt WS. An investigation on platelet transport during thrombus formation at micro-scale stenosis. *PLoS One*. 2013;8(10):e74123. <https://doi.org/10.1371/journal.pone.0074123> PMID: 24194822
57. Du J, Fogelson AL. A computational investigation of occlusive arterial thrombosis. *Biomech Model Mechanobiol*. 2024;23(1):157–78. <https://doi.org/10.1007/s10237-023-01765-8> PMID: 37702979
58. Bouchnita A, Belyaev AV, Volpert V. Multiphase continuum modeling of thrombosis in aneurysms and recirculation zones. *Phys Fluids*. 2021;33(9):093314. <http://dx.doi.org/10.1063/5.0057393>
59. Carminita E, Tourn J, Crescence L, Brouilly N, Alexandra GMs, Christophe M, et al. A thrombus is formed by a gradient of platelet activation and procoagulant endothelium. *Res Pract Thromb Haemost*. 2023;7(7):102209. <https://doi.org/10.1016/j.rpth.2023.102209> PMID: 38077809
60. Rana A, Westein E, Niego B, Hagemeyer CE. Shear-dependent platelet aggregation: Mechanisms and therapeutic opportunities. *Front Cardiovasc Med*. 2019;6:1–21. <https://doi.org/10.3389/fcvm.2019.00141> PMID: 31620451
61. Du J, Aspray E, Fogelson A. Computational investigation of platelet thrombus mechanics and stability in stenotic channels. *J Biomech*. 2021;122:110398. <https://doi.org/10.1016/j.jbiomech.2021.110398> PMID: 33933859
62. Babushkina ES, Bessonov NM, Ataullakhanov FI, Panteleev MA. Continuous modeling of arterial platelet thrombus formation using a spatial adsorption equation. *PLoS One*. 2015;10(10):e0141068. <https://doi.org/10.1371/journal.pone.0141068> PMID: 26517377
63. Belyaev, Aleksey V., Mikhail A. Panteleev, and Fazly I. Ataullakhanov. Threshold of microvascular occlusion: Injury size defines the thrombosis scenario. *Biophys J*. 2015;109(2):450–6. <https://doi.org/10.1016/j.bpj.2015.06.019> PMID: 26200881